AFRL-AFOSR-VA-TR-2020-0107

Waveguide Lasers and Phased Arrays Emitting in the Ultraviolet to Mid-Wave Infrared (MWIR) Spectral Regions

J Gary Eden
UNIVERSITY OF ILLINOIS

07/16/2020
Final Report

Air Force Research Laboratory
AF Office Of Scientific Research (AFOSR)/ RTB1
Arlington, Virginia 22203
Air Force Materiel Command

DISTRIBUTION A: Distribution approved for public release.

REPORT DOCUMENTATION PAGE

Form Approved
OMB No. 0704-0188

1. REPORT DATE *(DD-MM-YYYY)*	2. REPORT TYPE	3. DATES COVERED *(From - To)*
24-07-2020	Final Performance	01 Nov 2013 to 31 Oct 2019

4. TITLE AND SUBTITLE
Waveguide Lasers and Phased Arrays Emitting in the Ultraviolet to Mid-Wave Infrared (MWIR) Spectral Regions

5a. CONTRACT NUMBER

5b. GRANT NUMBER
FA9550-14-1-0002

5c. PROGRAM ELEMENT NUMBER
61102F

6. AUTHOR(S)
J Gary Eden

5d. PROJECT NUMBER

5e. TASK NUMBER

5f. WORK UNIT NUMBER

7. PERFORMING ORGANIZATION NAME(S) AND ADDRESS(ES)
UNIVERSITY OF ILLINOIS
506 S WRIGHT STREET SUITE 364
URBANA, IL 61801-3649 US

8. PERFORMING ORGANIZATION REPORT NUMBER

9. SPONSORING/MONITORING AGENCY NAME(S) AND ADDRESS(ES)
AF Office of Scientific Research
875 N. Randolph St. Room 3112
Arlington, VA 22203

10. SPONSOR/MONITOR'S ACRONYM(S)
AFRL/AFOSR RTB1

11. SPONSOR/MONITOR'S REPORT NUMBER(S)
AFRL-AFOSR-VA-TR-2020-0107

12. DISTRIBUTION/AVAILABILITY STATEMENT
A DISTRIBUTION UNLIMITED: PB Public Release

13. SUPPLEMENTARY NOTES

14. ABSTRACT

This AFOSR grant, initiated by Dr. Howard R. Schlossberg in 2014, has been dedicated to the pursuit of new sources of optical and UV/VUV radiation and their applications. We are pleased to report to AFOSR that the past five years of research have proven to be quite productive, yielding several developments that appear to be of significant value to the Air Force. Highlights of this research program include:
1. The conception and development of a laser whose output comprises literally thousands of microlaser beams. In the far field, these beams combine to form a single beam of low coherence and virtually no speckle. Such a laser has been pursued for decades by the optical community and is ideal for high spatial and temporal resolution LIDAR.
2. The discovery and development of biomolecular lasers, including R-Phycoerythrin and Flavin Mononucleotide. Both are compatible with human tissue and open the door to microlasers suitable for biomedical diagnostics within the human body

15. SUBJECT TERMS

16. SECURITY CLASSIFICATION OF:			17. LIMITATION OF ABSTRACT	18. NUMBER OF PAGES	19a. NAME OF RESPONSIBLE PERSON
a. REPORT	b. ABSTRACT	c. THIS PAGE			ROACH, WILLIAM
Unclassified	Unclassified	Unclassified	UU		19b. TELEPHONE NUMBER *(Include area code)* 703-696-7302

FINAL PERFORMANCE REPORT
FOR AFOSR GRANT
NO. FA9550-14-1-0002

"WAVEGUIDE LASERS IN THE VISIBLE AND ULTRAVIOLET"

Prepared For

Dr. William P. Roach
U.S. Air Force Office of Scientific Research
One Liberty Center
875 North Randolph Street
Arlington, VA 22203-1768

Submitted By

J. Gary Eden
Andrey E. Mironov
University of Illinois
Department of Electrical and Computer Engineering
306 North Wright Street
Urbana, IL 61801

July 2020

I. INTRODUCTION AND SUMMARY OF ACCOMPLISHMENTS

This AFOSR grant, initiated by Dr. Howard R. Schlossberg in 2014, has been dedicated to the pursuit of new sources of optical and UV/VUV radiation and their applications. We are pleased to report to AFOSR that the past five years of research have proven to be quite productive, yielding several developments that appear to be of significant value to the Air Force. Highlights of this research program include:

1. The conception and development of a laser whose output comprises literally thousands of microlaser beams. In the far field, these beams combine to form a single beam of low coherence and virtually no speckle. Such a laser has been pursued for decades by the optical community and is ideal for high spatial and temporal resolution LIDAR.
2. The discovery and development of biomolecular lasers, including R-Phycoerythrin and Flavin Mononucleotide. Both are compatible with human tissue and open the door to microlasers suitable for biomedical diagnostics within the human body.
3. Demonstration of the first dynamic, 3D plasma photonic crystals and their operation in the 100-300 GHz region. These crystals have been shown to be well-suited for communications in the mm-wave and THz spectral regions as dynamic filters, reflectors, and resonators for large bandwidth, multichannel communications. We believe these devices will enable new communications systems in this important spectral region.
4. The first observation of laser fractal modes. Such modes are fundamentally different from the Gaussian modes on which lasers have invariably relied upon for decades.
5. Demonstration of lamp-driven photolithography at 172 nm. Features as small as 350 nm have been fabricated in polymers with a VUV lamp developed with Illinois microplasma technology.
6. Discovery and development of microplasma-assisted atomic layer deposition (MALD).
7. Efficient and scalable alkali-rare gas lasers in the 780-852 nm region have been developed.

In addition to these technical accomplishments, 29 U.S. and international patents have been received during this grant. Every one of these patents acknowledges AFOSR as the sole supporter of the results being patented. Finally, technical articles have been published in high quality journals as a result of this grant. Once again, each article credits AFOSR as the source of support.

II. BRIEF DESCRIPTION OF SEVERAL HIGHLIGHTS

In this section, a few of the highlights listed above are described briefly. Details regarding these and other accomplishments can be found in the publications listed in Section III.

A. Laser Resonator Emitting Fractal Modes and Multiple Beams

One of the major accomplishments realized in this research program is the demonstration of a new form of laser resonator that is capable of emitting fractal laser modes and beams comprising literally thousands of microlaser beams. The concept of embedding micro-refractive elements in conventional laser resonators has been studied extensively throughout the duration of this grant and has resulted in several entirely new resonator architectures. By pixelating the transverse plane of a two-mirror optical resonator with arrays of microspheres or commercial microlenses (Fig. 1), a single millimeter-scale cavity can produce hundreds or thousands of separate laser beams. Hermite-Gaussian, Laguerre-Gaussian, and Ince-Gaussian transverse modes with indices ranging from zero to more than 30 have been observed routinely. In addition, numerous "hybrid modes" have been observed that have not been reported previously in the literature, presenting the possibility of generating new modes that are well-suited for specific propagation, sensing, or optical trapping applications.

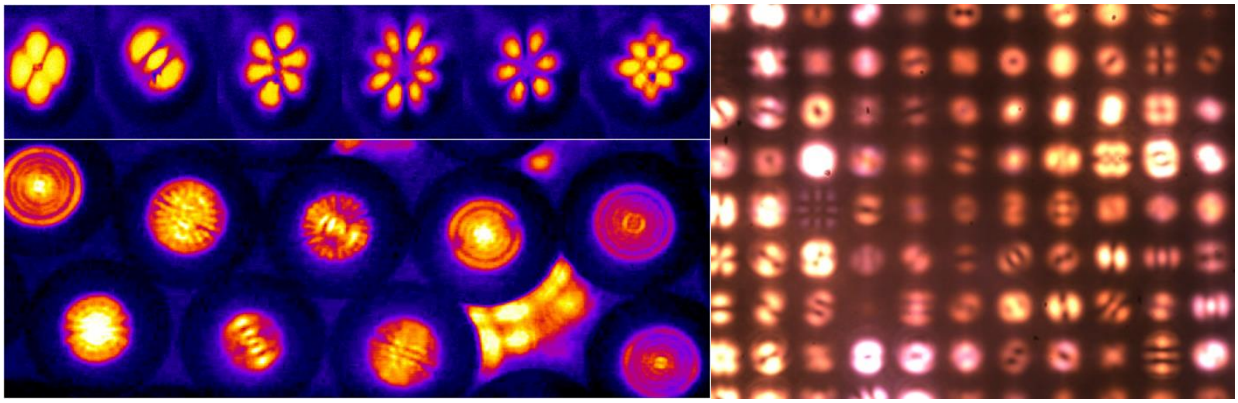

Fig. 1. A variety of low- and high-order transverse modes obtained from Fabry-Pérot laser resonators stabilized by microspheres (left) and a commercial lens array (right). The spheres can be readily assembled into large arrays consisting of hundreds or thousands of individual beams.

Instead of limiting experiments to only static, inanimate lenses, living cells were also used to pixelate the optical resonator. Laser oscillation was observed when *Chlamydomonas reinhardtii*—a single-cell, phototactic algae—stabilized a dual-chamber optical cavity after moving into the active volume (Fig. 2). Because the laser resonant mode profile is sensitively dependent on refractive index variations of the lens, real-time phase information of the organism can, in principle, be extracted from information encoded in the laser emission spatial profile.

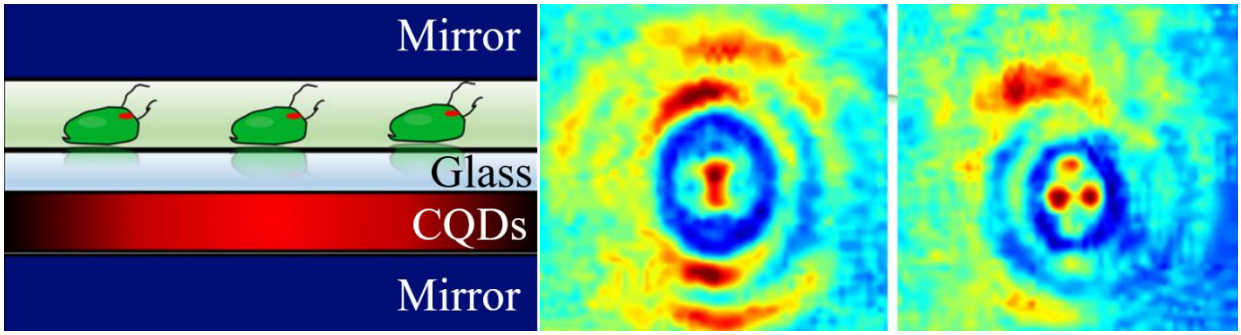

Fig. 2. *C. reinhardtii* algae acting as a stabilizing lens inside a dual-chamber laser cavity.

A key feature of this new laser resonator is that a Gaussian laser beam is generated at every microsphere (or other refractive element) in the array situated within the laser resonator. Consequently, beams produced by these optical cavities comprise literally thousands of microlaser beams from a common aperture. Such a laser is much more than a laboratory curiosity, however, because the phases of the individual microlaser beams vary randomly with respect to those of the other microlasers. The result is that the composite laser beam is completely incoherent and, thus, free of speckle. That is, this new optical source is a laser in every respect except that its phase properties are those of an incoherent source. Many research groups have pursued the development of a speckle-free laser sources for more than 5 decades. Unfortunately, all of these efforts have been of limited success and many have relied on mechanical solutions. The laser developed under this AFOSR grant allows for the degree of coherence of the composite beam to be varied continuously by simply varying the number of microlaser beams contributing to the whole. Figure 3 is a photograph of the rotor in a turbomolecular vacuum pump that has been imaged with an array of more than 2000 microlaser beams. The laser array was pumped by the ~8 ns pulses produced by a frequency-doubled, Q-switched Nd:YAG laser. Although the pump is in operation and rotating at more than 50,000 rpm, the image of Fig. 3 is free of motion blur and offers a spatial resolution of ~100 μm. The characteristics of this imaging laser are far superior to those of past

"speckle-free" sources (such as random lasers) and we recommend that this laser be employed for imaging high speed phenomena of interest to the Air Force such as operating jet engines. With this new tool, it may be possible to diagnose jet engines while in the field. That is, engines can be observed under full operating load, allowing for mechanical stress or impending failure to be observed directly without the need for removing the aircraft from service. Consequently, this laser could significantly reduce the cost and time normally required for periodic inspection of jet engines.

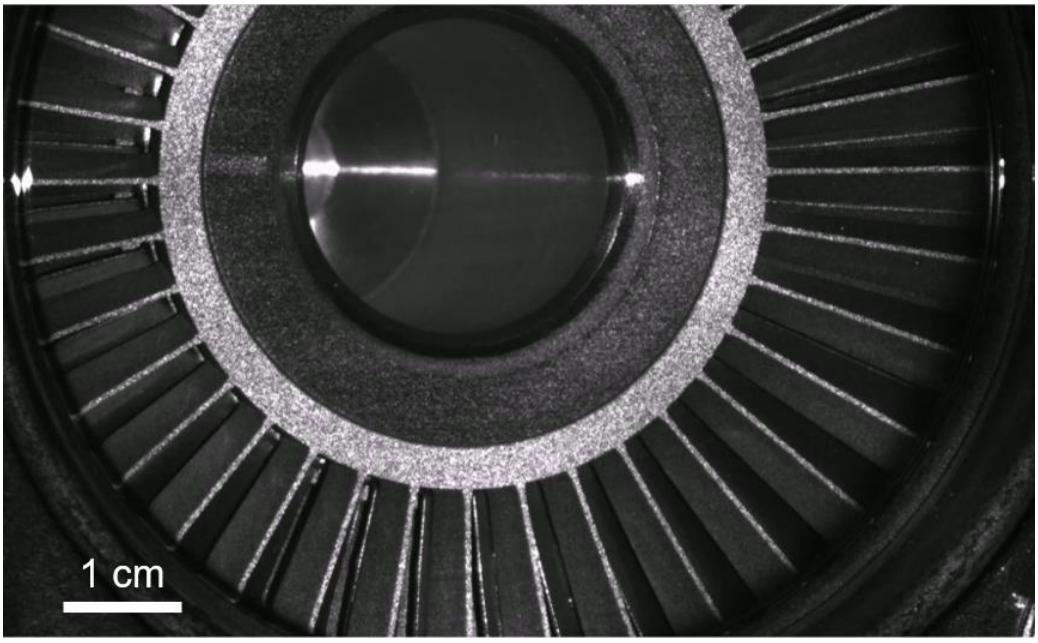

Fig. 3. Optical image of a turbomolecular vacuum pump, operating at 50,000 rpm and viewed from a distance of 2.5 m. Notice the absence of motion-blur because this image was recorded with a single, ~8 ns pulse from a speckle-free laser comprising more than 2000 microlasers.

B. Efficient Alkali-Rare Gas Lasers and Amplifiers Operating in the 780-852 nm Spectral Region

Our laboratory has conducted spectroscopic studies of alkali-rare gas mixtures for a number of years and, during this AFOSR grant, we have leveraged that experience to demonstrate a new family of alkali-rare gas lasers that operate in the near-infrared region. For the sake of brevity, Fig. 4 shows data for a Cs-Ar laser system normally pumped at 836.7 nm, the peak of the blue satellite of the D2 line in Cs-Ar mixtures. This vapor-phase amplifier is pumped by the photoassociation of Cs and Ar atomic pairs, and power is extracted efficiently from the

electronically-excited, Cs-Ar* diatomic complex. The pump and probe beams are nanosecond pulses with durations of 8 ns and the two beams are spatially and temporally overlapped. A Cs-Ar cylindrical gas cell has a gain length of 10 cm and the pump and probe beams traverse the cell only once. As shown in the gain spectrum on the right side in Fig. 4, optical amplification occurs over ~0.4 nm on the red wing of Cs D_2 line. The broadening of the gain spectrum results from the interatomic potential curves, not the result of pressure broadening of the resonance line which is on the order of 0.01 nm (FWHM). The circular polarization of the pump and probe beam allows the effective population inversion to be increased and, consequently, raises the gain by 20% even after compensating for the loss by two quarter-wave plates. The curve on the right side in Figure 4 shows the amplifier efficiency versus pump energy. At the pump energy of 5 mJ, the optical-to-optical efficiency reaches 28% and the corresponding total efficiency is 11 %.

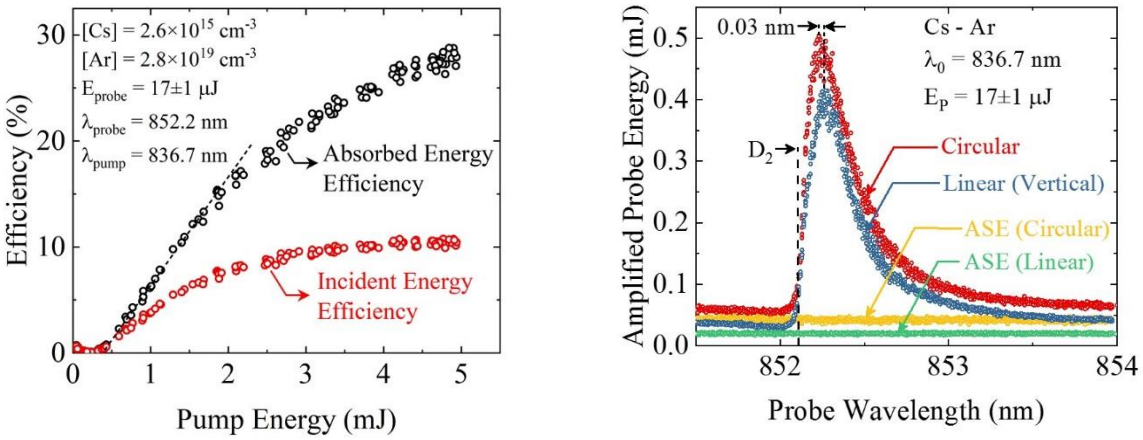

Fig. 4. (Left) Amplified probe pulse energy shown versus the pump pulse energy. (Right) The gain spectrum exhibits a large bandwidth of over ~0.4 nm (160 GHz), and peaking at 852.2 nm. It also shows the dependence of the amplified pulse energy on the light polarization.

C. Discovery and Development of Biomolecular Lasers

Another major accomplishment realized under this AFOSR program is the discovery and development of biomolecular lasers, and particularly those that are compatible with human tissue. The first laser investigated was flavin mononucleotide (FMN) which is a derivative of Vitamin B_2. The FMN laser cavity consisted of a Fabry-Perot cavity with a mirror spacing of 375 μm. This cavity was pumped with a pulsed, frequency-tripled Nd:YAG laser. The spectrum for FMN in

water with a pump energy density of 300 μJ/mm^2 is shown below in Figure 5. The FSR for the optical cavity was 0.325 nm which is consistent with the cavity spacing.

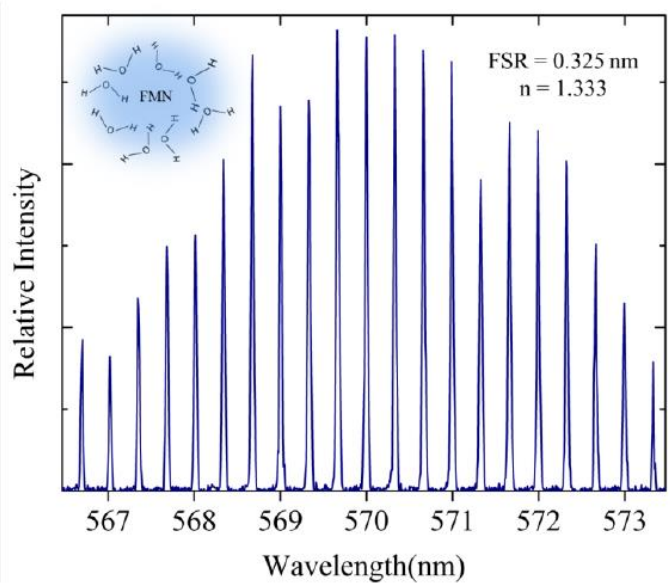

Fig. 5. Laser spectrum for FMN and water as the solvent. However, when the solvent for FMN is changed to a 1:3 ratio of FMN/glycerol/water, a noticeable blue shift occurs in the spectrum as shown in blue in Fig. 6 presented below. The red curve in Figure 6 is the FMN/water spectrum, shown for reference. The FSR of the new solvent with FMN is 0.302 nm for n=1.42913 which is the refractive index for this particular mixture of glycerol and water at room temperature.

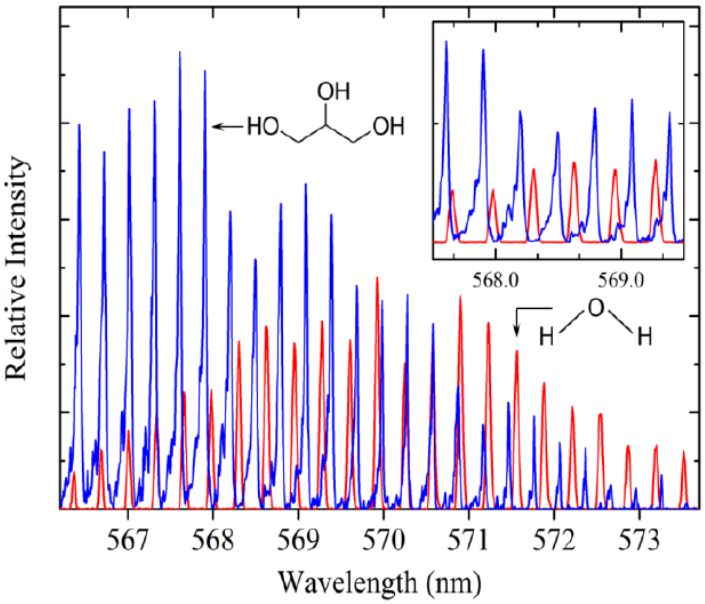

Fig. 6. Laser spectra for 1:3 solutions of FMN/glycerol/water (blue) and FMN/water (red). The inset is a magnified portion of the spectra. It can be seen that the glycerol introduces transverse mode structure due to the microbubbles in the new solution which act as microlenses. As a result, the Hermite-Gaussian modes are no longer degenerate.

The laser spectrum obtained from the fluorescent protein known as R-Phycoerythrin is shown in Fig. 7 below. This biomolecule is a member of the phycobiliproteins, which are fluorescent protein pigments from blue-green and red algae. When extracted from the algae, phycobiliproteins can retain their high absorbance and fluorescence in solution due to the dense packing of chromophores. In this laser system, the phycobiliprotein subunit lies inside the protein R-phycoerythrin. This protein was placed inside a Fabry Perot cavity of spacing 777 μm and was pumped by the second harmonic of a pulsed, nanosecond Nd:YAG laser. The pump energy density threshold for this laser was ~197 μJ/mm^2 and the peak energy was about 27 nJ. The spectrum for this laser is given in Figure 7 which clearly shows 112 longitudinal modes separated by 0.18 nm when pumped with an energy density of ~600μJ/mm^2. These results represent the first demonstration of lasing from a fluorescent protein pigment.

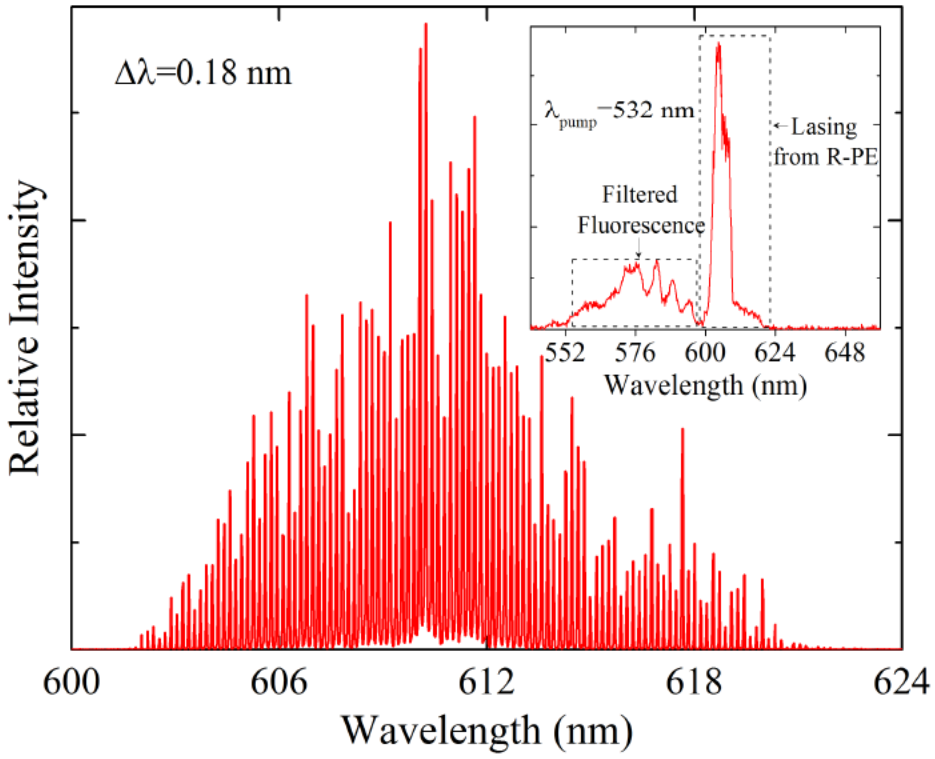

Fig. 7. R-phycoerythrin laser spectrum observed when the molecule is pumped at about three times above threshold. The 0.18 nm mode spacing corresponds to the cavity length of 777 μm. The inset is a low-resolution spectrum that does not show longitudinal mode structure.

Similar experiments with Red Fluorescent Protein (RFP) yielded the extensive laser spectrum shown in Fig. 8. Fluorescent proteins serve as an important tool in biology. Specifically, these proteins play a significant role in bio-imaging and help understand the study of *in vivo* biomolecular processes. Using a mCherry recombinant as the red fluorescent protein for the gain media in a Fabry Perot cavity with a mirror separation of 740μm and pumping it with a frequency double pulsed nanosecond Nd:YAG laser, the spectrum of Fig. 8 was obtained. In this spectrum, 128 longitudinal modes were observed, and lasing threshold was measured to be about 200 $\mu J/mm^2$. These findings contain the highest number (by far!) of the longitudinal modes observed for any biological laser. The frequency comb in Fig. 8 can allow for monitoring protein biomolecular interactions.

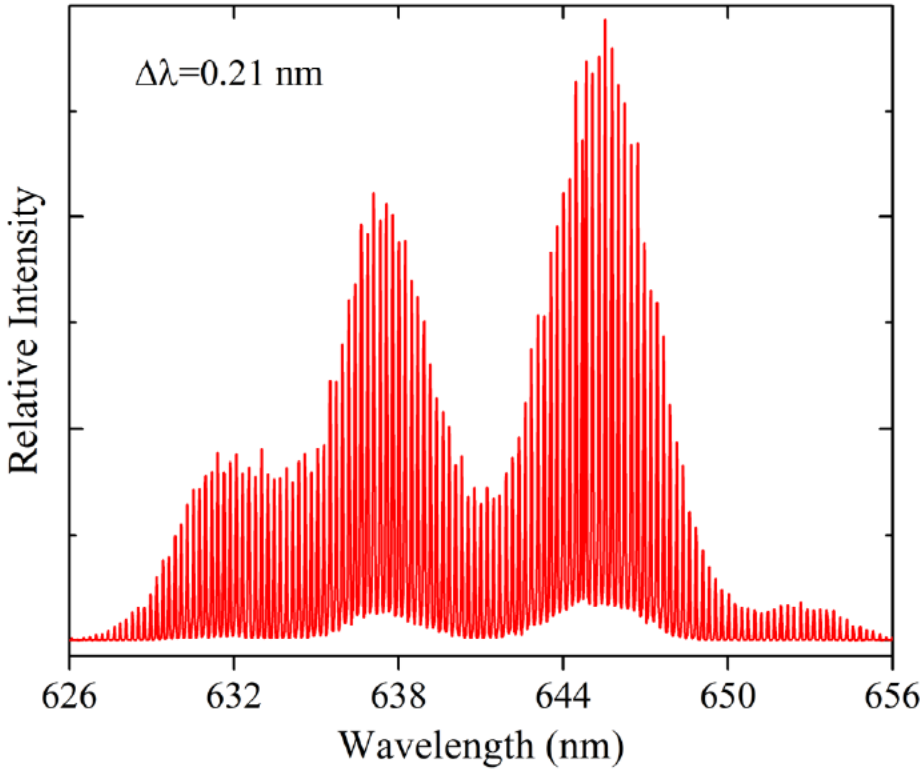

Fig. 8. Laser spectrum for RFP in the 626 – 656 nm region. More than 120 longitudinal modes are clearly observed.

D. FRET Laser Using Biotin-Streptavidin Bioconjugates

Förster resonance energy transfer (FRET) was first demonstrated in the 1960s as a spectroscopic ruler at the nanometer scale by measuring the energy transfer from a donor molecule to an acceptor molecule. This approach was applied to the donor-acceptor pair biotin-streptavidin, a conjugate system offering one of the strongest known non-covalent interactions. The laser cavity used Cy3-Streptavidin and Cy5-Biotin as the gain medium with a ratio of 2.25 between the acceptor and the donor. The protein-ligand pairs were placed in a Fabry-Perot cavity with a mirror separation of 1.2 mm and were also pumped with a pulsed Nd:YAG laser at 532nm. The spectrum for this is shown in black in Figure 9.

In order to reduce the acceptor-donor ratio, the Cy5-Biotin complex was replaced by biotinylated gold nanoparticles and the acceptor-donor ratio was decreased to 10^{-7}. This reduction in the acceptor-donor ratio corresponds to a higher FRET efficiency. The laser spectrum for this is shown in Fig. 9. As one can see, there is a red-shift in the lasing spectrum which is consistent with the surface plasmon resonance peak of the 100 nm gold nanoparticles.

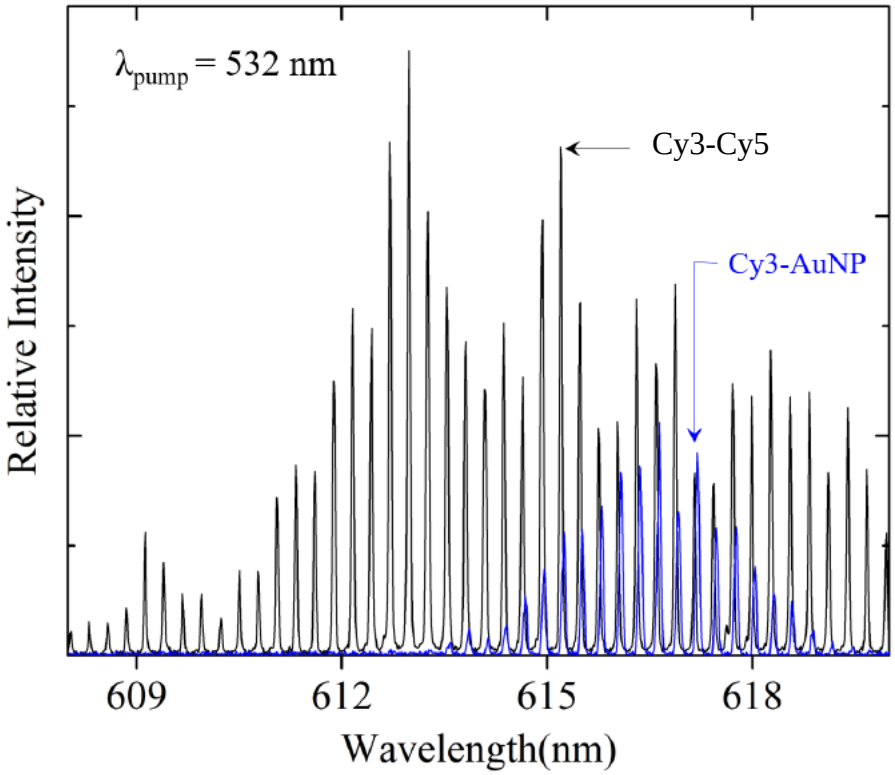

Fig. 9. Laser spectra for the biotin-streptavidin FRET laser. The replacement of Cy5 with gold nanoparticles (AuNP) red shifts and attenuates the original lasing spectrum. Replacing Cy5 with Au nanoparticles resulted in a decrease in the acceptor-donor ratio and an increase in the pump threshold. The threshold energy for the Cy3-Cy5 was ~75 μJ/mm^2 while the Cy3-AuNp threshold pump energy density was ~115 μJ/mm^2.

E. Photolithography and Photopatterning at 172 nm

Perhaps the most significant achievement of this AFOSR program is the discovery and commercialization of a novel photolithographic technique utilizing flat microplasma lamps emitting 172 nm radiation. This process allows for low cost, high resolution patterning of most known polymers such as PMMA, PDMS, polycarbonates and many others. Complex, 3D structures having features sizes of ~350 nm and below can now be directly etched into polymers using the demonstrated technique, and optical elements such as gratings, phase masks, and Fresnel lenses are easily fabricated. Figures 10 and 11 (shown below) present images of a Fresnel lens and a complex nanostructure, respectively, both of which were fabricated in a polymer surface with a 172 nm exposure system. This technology has now been commercialized through the formation of a company known as Cygnus Photonics. Manufacturing began more than 1.5 years ago and multiple units similar to that shown in Fig. 12 have been sold worldwide.

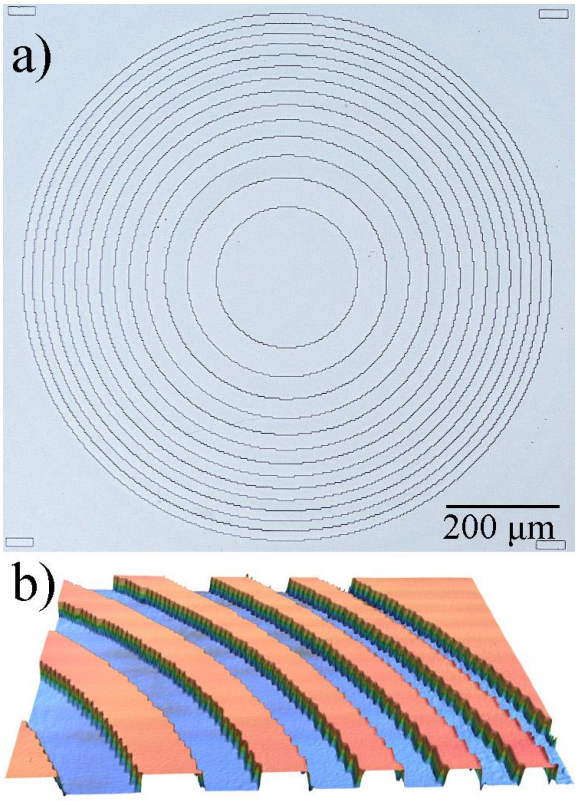

Fig. 10. (a) Optical image in plan view of a Fresnel lens fabricated in a polymer by 172 nm photolithography, and (b) laser confocal profilometer image of a section of the lens. The overall diameter of the lens structure is 1 mm and its focal length is 50 mm.

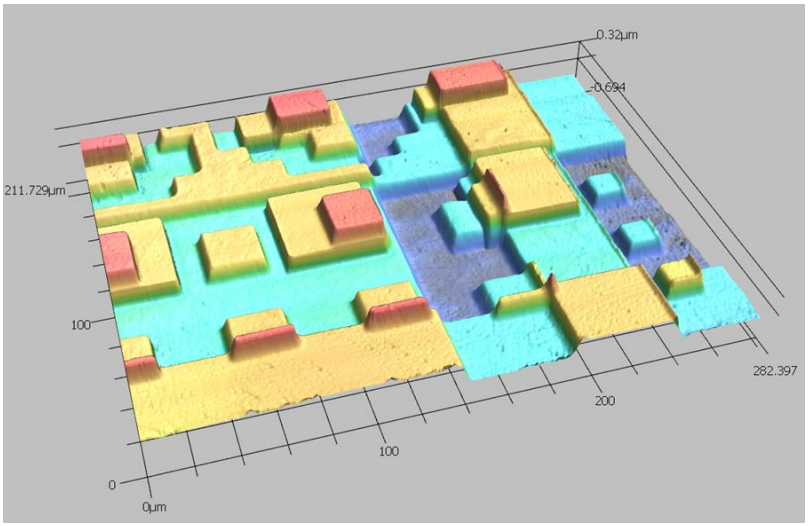

Fig. 11. Confocal laser profilometer scan of a complex nanostructure fabricated in the surface of an acrylic sheet by multiple exposures of the polymer surface with 172 nm radiation. Obtaining this structure required the rotation and translation of a single mask between exposures.

Fig. 12. Photograph of a compact 172 nm exposure system for fabricating patterned polymer films on Si. This system is currently being manufactured by Cygnus Photonics of Champaign, IL, a company formed as a result of this AFOSR program.

F. Microplasma-Assisted Atomic Layer Deposition (MALD)

The last highlight of this AFOSR program that will be described here is the demonstration of a new process for depositing nanoscale films by Atomic Layer Deposition (ALD). Figure 13 shows diagrams of microplasma arrays that have been developed for the purpose of dissociating the precursors responsible for film growth. Experiments to date have focused on the growth of aluminum oxide when trimethylaluminum (TMA) and oxygen serve as precursors, and Fig. 14 presents scanning electron micrographs (SEMs) of alumina films grown onto patterned substrates. Conformal films are grown on the side-walls of steep trenches, even for FIB-fabricated trenches more than 3 um in depth. Figure 15 shows cross-sectional TEM images of the Si/silicon oxide/alumina interface for films grown at 50 °C and with an 800 °C post-anneal process.

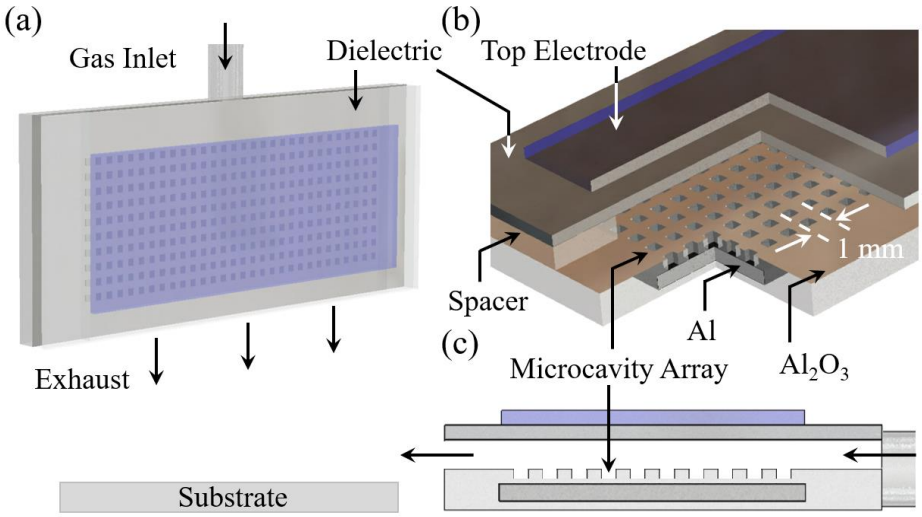

Fig. 13. Diagrams of the 50 × 20 microcavity plasma array and enclosure: (a) Diagram of the assembled array structure, showing the precursor inlet tube at top, and the exhaust exiting downward. A quartz window allows for the fluorescence from the microplasmas to be observed; (b) Cutaway view of the array structure (not to scale), illustrating the fabrication of the square microcavities in nanoporous Al_2O_3 and the array pitch of 1 mm; (c) Cross-sectional diagram of the array, indicating the flow of the O_2 precursor.

Because of the low film growth temperatures accessible with the MALD process, it is possible to grow high quality films onto low temperature substrates. Figure 16 shows photographs of arrays of gallium-oxide (Ga_2O_3) photodetectors fabricated on the polymer PET. The arrays are undergoing electrical tests in a probe station, and Fig. 17 presents several of the measurements of the photoresponse of the detectors, measured at several wavelengths in the deep-UV spectral region. The result of these studies is that the MALD-grown UV photodetectors have characteristics

(responsivity, dark noise, etc.) superior to those of detectors based on films grown by conventional ALD.

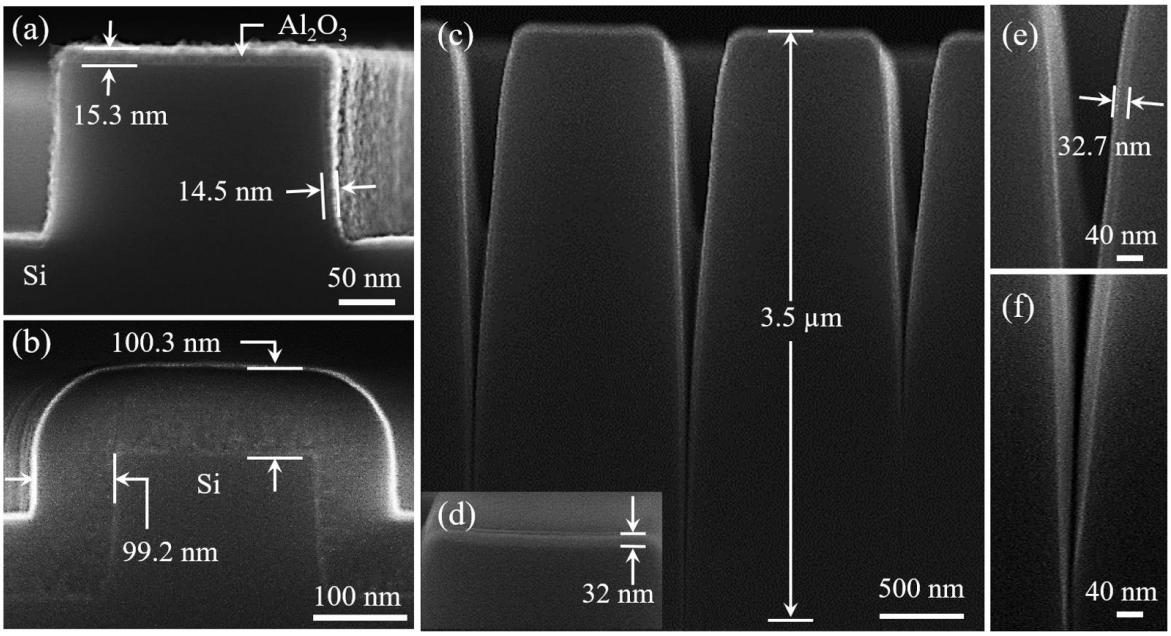

Fig. 14. Scanning electron microscopy (SEM) images of Al_2O_3 nanofilms grown onto periodic ridges and trenches in Si substrates. (a) SEM image of ~ 15 nm thick Al_2O_3 film, grown onto the surface of a Si(100) wafer as well as into two adjacent trenches, and viewed slightly off the axis of the resulting ridge; (b) End-on view of a single Si ridge onto which a 100 ± 0.8 nm-thick alumina film has been deposited at 50 °C by MALD; (c) Low resolution electron micrograph of a portion of an FIB-machined series of tapered trenches fabricated in Si. A ~ 32 nm-thick Al_2O_3 film has been grown onto this periodic structure; (d) Expanded view of the surface of one ridge from (c), indicating the Al_2O_3 film thickness; (e) and (f) Magnified SEM views of two progressively-deeper portions of one trench in panel (c).

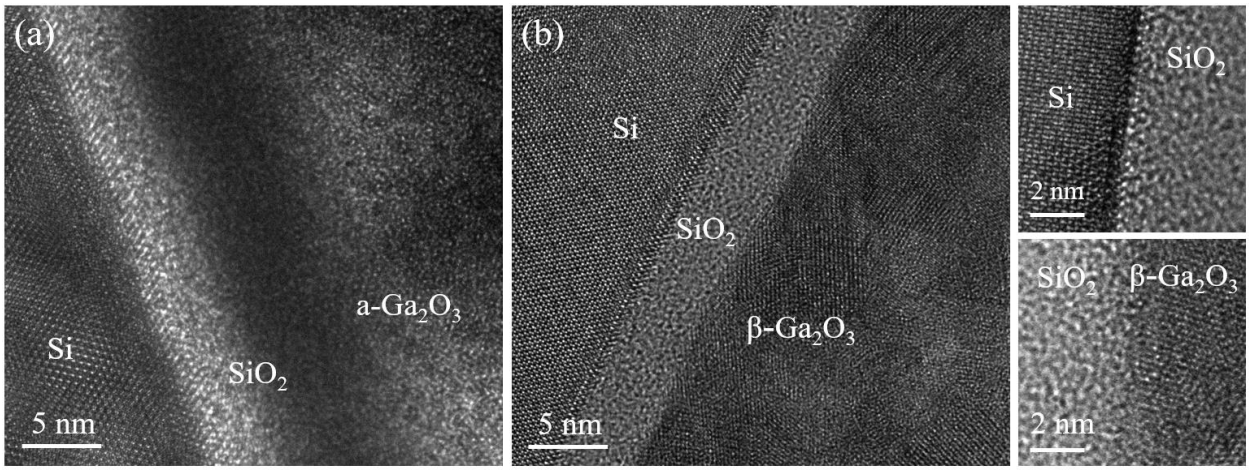

Fig. 15. (a) Cross-sectional TEM image of an amorphous Ga_2O_3 thin film grown on Si; (b) TEM of a polycrystalline β−Ga_2O_3 thin film grown on Si with a post-anneal at 800 °C.

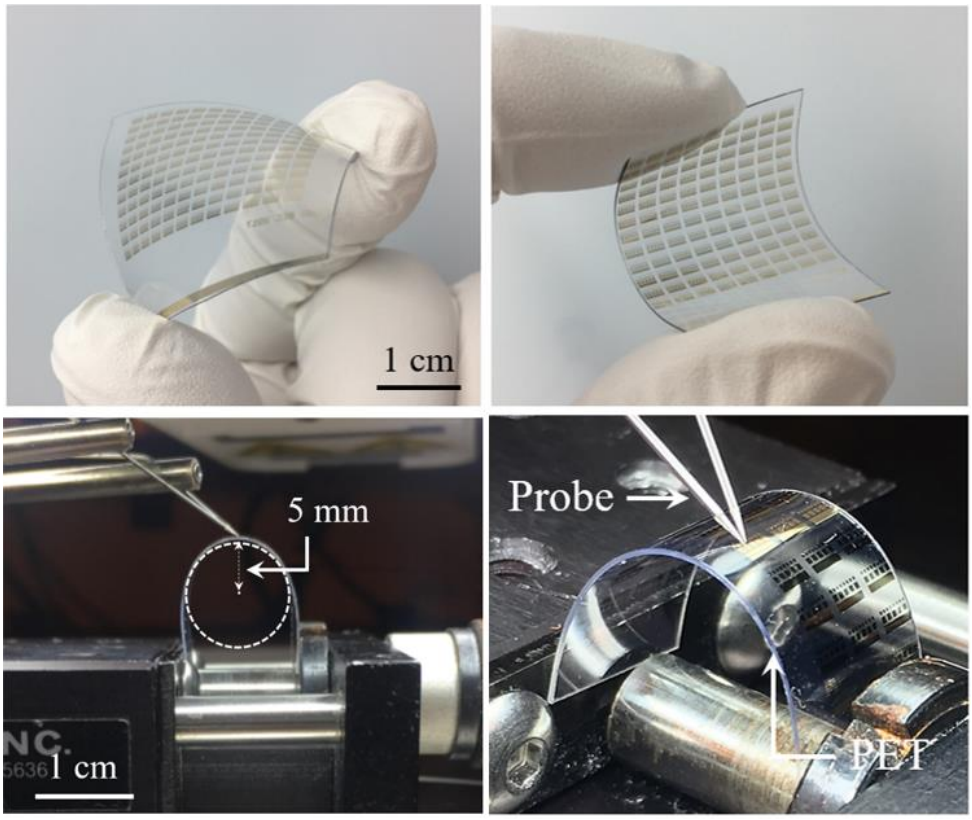

Fig. 16. Photographs of flexible DUV photodetector arrays with a convex/concave curvature, undergoing testing in a probe station. The substrate is PET (plastic).

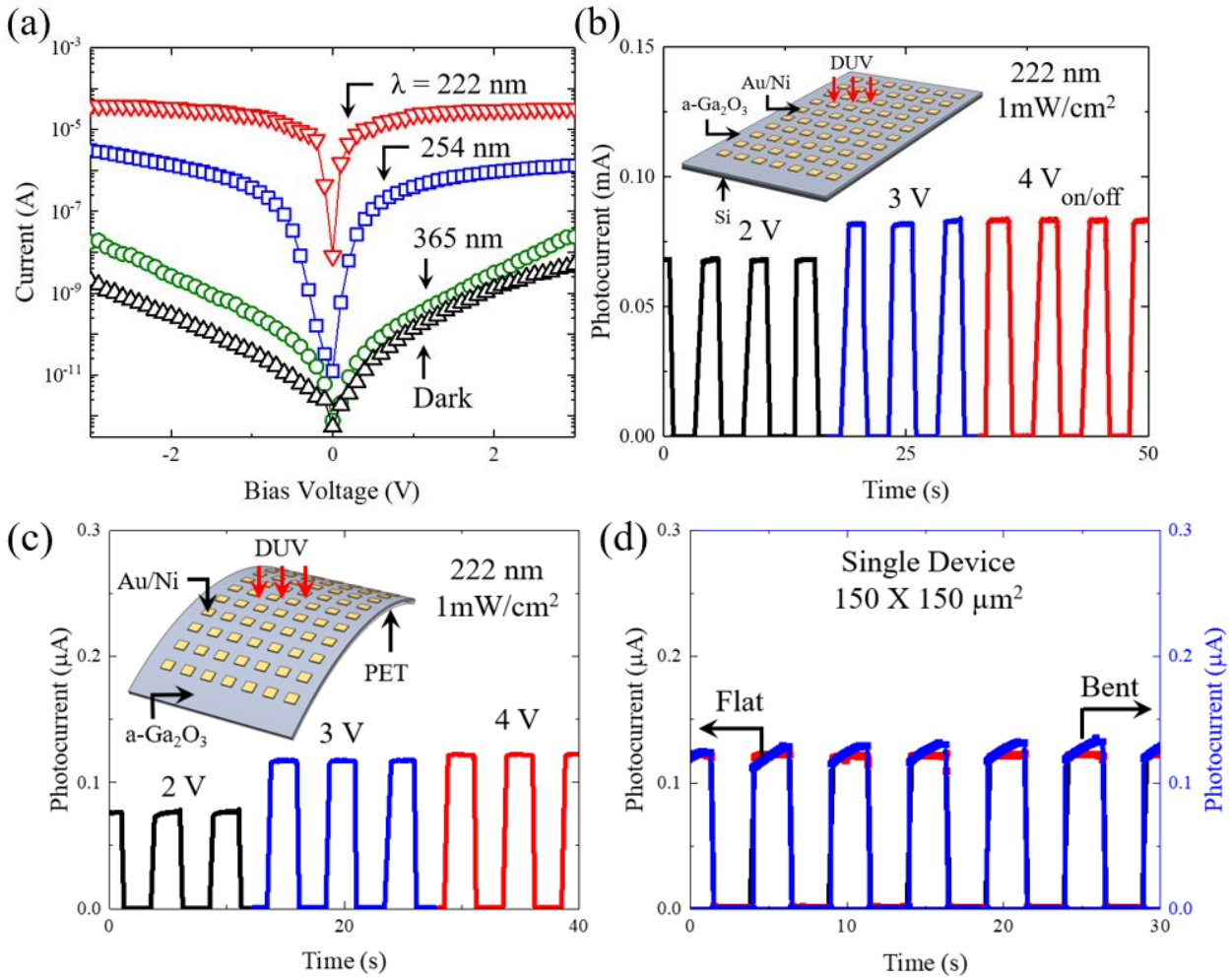

Fig. 17. (a) I-V characteristics of metal/Ga_2O_3/metal (MSM) film structures, designed for DUV photodetectors, in the dark, and under 365 nm, 254 nm and 222 nm light irradiation; (b) Time-dependent photoresponse of the MSM structure based a-Ga_2O_3/Si films under 222 nm UV illumination with 2.5 s on/off period (b) Time dependent photoresponse of a-Ga_2O_3/PET based MSM structure under 222 nm UV illumination with 2.5 s on/off period. (c) Measurement of photodetector performance under 222 nm illumination before and after bending the photodetector with a bending radius of 5 mm.

III. PAPERS PUBLISHED UNDER AFOSR GRANT NO. FA9550-14-1-0002

The scientific articles published as a result of this AFOSR program are listed in this section. All of these publications acknowledge AFOSR as the sole source of support for the work described.

1. K.E. Keister, C.J. Wagner, J.L. Putney, J.D. Hewitt, and J.G. Eden, "Determination of Ar_2^+ and N_4^+ recombination coefficients by subpicosecond multiphoton ionization at 248 nm and microwave interferometry," Phys. Rev. A, vol. 89, 013401 (2014).
2. W.-J. Kuang, Q. Li, H. Tolner, T. Oh, S.-J. Park, and J. G. Eden, "Large area polymeric microplasma devices with elongated lifetime for flexible display and photonic applications," IEEE Electron Device Lett., vol. 35, pp. 765-767 (July 2014).
3. C. J. Wagner, T. C. Galvin, and J. G. Eden, "Xe_2 gerade Rydberg states observed in the afterglow of a microplasma by laser spectroscopy of $\alpha^3\Sigma^+_u$ (1u, 0-u) absorption in the green (545-555 nm) and near infrared (675-800 nm)," J. Chem. Phys., vol. 140, 244312 (2014).
4. M. R. Gartia, S. Seo, J. Kim, T.-W. Chang, G. Bahl, M. Lu, G. L. Liu, and J. G. Eden, "Injection-seeded optoplasmonic amplifier in the visible," Sci. Reports, vol. 4, 6168 (August 26, 2014); DOI:10.1038/srep06168.
5. C. H. Park, J. S. Lee, J. H. Kim, D.-K. Kim, O. J. Lee, H. W. Ju, B. M. Moon, J. H. Cho, M. H. Kim, P. P. Sung, S.-J. Park, and J. G. Eden, "Wound healing with nonthermal microplasma jets generated in arrays of hourglass microcavity devices," J. Phys. D: Appl. Phys., vol. 47, 435402 (October 29, 2014).
6. A. E. Mironov, W. Goldshlag, and J. G. Eden, "Two color pumping of the Rb D2 line laser (780 nm) through the photoassociation of Rb-Ar or Rb-Xe thermal pairs: Realization of a quantum efficiency above one," Appl. Phys. Lett., vol. 107, 041112 (2015).
7. H. Cheng, A. E. Mironov, J. H. Ni, H. J. Yang, W. W. Chen, Z. Dai, P. D. Dragic, J. Dong, S.-J. Park and J. G. Eden, "Coupling quantum dots to optical fiber: Low pump threshold laser in the red with a near top hat beam profile", Appl. Phys. Lett., vol. 106, 081106 (2015).
8. O. J. Lee, H. W. Ju, G. Khang, P. P. Sun, J. Rivera, J. H. Cho, S.-J. Park, J. G. Eden, and C. H. Park, "An experimental burn wound-healing study of non-thermal atmospheric pressure microplasma jet arrays," J. Tissue Eng. Regen. Med. (2015); DOI:10.1002/term.
9. P. P. Sun, H. L. Chen, S.-J. Park, J. G. Eden, D. X. Liu, and M. G. Kong, "Off-axis chemical crosstalk in an atmospheric pressure microplasma jet array," J. Phys. D: Appl. Phys., vol. 48, 425203 (2015).
10. T. C. Galvin, C. J. Wagner, and J. G. Eden, "Interruption of electronically excited Xe dimer formation by the photoassociation of Xe 6s[3/2]2 – Xe (5p6 1S0) thermal collision pairs," J. Chem. Phys., vol. 144, 244308 (2016).
11. J. A. Rivera and J. G. Eden, "Flavin mononucleotide biomolecular laser: longitudinal mode structure, polarization, and temporal characteristics as probes of local chemical environment", Opt. Express, vol. 24, pp. 10858-10868 (2016).

12. Y. Wang, J. H. Ni, S. Zhong, X. Zhang, Z. Liang, C. Liu, S.-J. Park, and J. G. Eden, "Microplasma mode transition and corresponding propagation characteristics controlled by manipulating electric field strength in a microchannel-cavity hybrid structure device", J. Phys. D: Appl. Phys., vol. 49, 415206 (2016).
13. Y. Wang, J. H. Ni, S. Zhong, S. Cai, X. Zhang, C. Liu, S.-J. Park, and J. G. Eden, "Perturbation and coupling of microcavity plasmas through charge injected into an intervening microchannel", J. Appl. Phys., vol. 120, 183303 (2016).
14. A. Semnani, H. J. Yang, M. Sinanis, S.-J. Park, J. G. Eden, S. O. Macheret, and D. Peroulis, "Low temperature plasma for tunable resonant attenuation", Proc. IEEE Microwave Symposium (MTT-S) (2016); DOI: 10.1109/MWSYM.2016.7540426.
15. A. Semnani, H. J. Yang, M. Sinanis, S.–J. Park, J. G. Eden, S. O. Macheret, and D. Peroulis, "Power limiting characteristics of a plasma-loaded evanescent-mode cavity resonator", Proc. 46th European Microwave Conference, pp. 627-630 (London, October 2016).
16. S. Dong, J. Li, M.-H. Kim, S.-J. Park, J. G. Eden, J. S. Guest, and T. H. Nguyen, "Human health trade-offs in the disinfection of wastewater for landscape irrigation: microplasma ozonation vs. chlorination", Environ. Sci.: Water Res. Technol., vol. 6, pp. 106-118 (2017); doi: 10.1039/c6ew00235h.
17. S.-J. Park, C. M. Herring, A. E. Mironov, J. H. Cho, and J. G. Eden, "25 W of average power at 172 nm in the vacuum ultraviolet from flat, efficient lamps driven by interlaced arrays of microcavity plasmas", APL Photonics, vol. 2, 041302 (March 8, 2017).
18. A. E. Mironov, J. D. Hewitt, and J. G. Eden, "Spin polarization of Rb and Cs np 2P3/2 (n=5,6) atoms by circularly-polarized photoexcitation of a transient diatomic molecule", Phys. Rev. Lett., vol. 118, 113201 (March 17, 2017).
19. M.-H. Kim, J. H. Cho, S.-J. Park, and J. G. Eden, "Modular and efficient ozone systems based on massively parallel chemical processing in microchannel plasma arrays: performance and commercialization", Eur. Phys. J. Special Topics, vol. 226, pp. 2923-2944 (2017); doi: 10.1140/epjst/e2016-60355-8.
20. H. Cheng, Y. Zhou, A. E. Mironov, W. Wang, T. Qiao, W. Lin, Q. Qian, S. Xu, Z. Yang, and J. G. Eden, "Mode suppression of 53 dB and pulse repetition rates of 2.87 and 36.4 GHz in a compact, mode-locked fiber laser comprising coupled Fabry-Perot cavities of low finesse (F=2)", Opt. Express, vol. 25, no. 20, pp. 24400-24409 (October 2, 2017); doi: 10.1364/OE 25.02440.
21. H. J. Yang, S.-J. Park, and J. G. Eden, "Narrowband attenuation at 157 GHz by a plasma photonic crystal", J. Phys. D: Appl. Phys., vol. 50, 43LTo5 (2017); doi:10.1088/1361-6463/aa8d5c.
22. A. E. Mironov and J. G. Eden, "Manipulating excited state hyperfine level populations in an atomic laser through electronic spin polarization: controlling upper laser level degeneracy and small signal gain", Opt. Exp., vol. 25, no. 24, pp. 29676-29686 (November 27, 2017).
23. J. A. Rivera and J. G. Eden, "Lasing at 602-620 nm from a red algae-derived phycobiliprotein", APL Photonics, vol. 2, 121301 (2017); doi:10.1063/1.4999716
24. H. J. Park, S. H. Kim, H. W. Ju, H. Lee, Y. Lee, S. Park, H. Yang, S.-J. Park, J. G. Eden, J. Yang, and C. H. Park, "Microplasma Jet Arrays as a Therapeutic Choice for Fungal Keratitis", Sci. Reports, vol. 8, 2422 (2018); doi:10.1038/s41598-018-20854-8.

25. S. K. Dong, J. Li, M.-H. Kim, J. H. Cho, S.-J. Park, T.H. Nguyen, and J. G. Eden, "Deactivation of Legionella Pneumophila in Municipal Wastewater by Ozone Generated in Arrays of Microchannel Plasmas", J. Phys. D: Appl. Phys., vol. 51, 255501 (June 1, 2018).
26. J. A. Rivera, T. C. Galvin, A. W. Steinforth, and J. G. Eden, "Fractal modes and multi-beam generation from hybrid microlaser resonators", Nature Commun., vol. 9, 2594 (July 3, 2018); doi: 10.1038/s41467-018-04945-8.
27. A. E. Mironov, D. L. Carroll, J. W. Zimmerman, and J. G. Eden. "Cs D2 line laser (852.1 nm) pumped by the photoassociation of Cs-Ar, Cs-Kr, and Cs-Xe collision pairs: Impact of rare gas partner on threshold and efficiency" App. Phys. Lett., vol. 113(5), 051105 (2018); https://doi.org/10.1063/1.5036995
28. T. C. Galvin and J. G. Eden, "Markov–Airy description of optical scattering, waveguides, and resonators," J. Opt. Soc. Am. A 36, 898-909 (2019)

IV. PATENTS GRANTED

All of the patents listed below issued during the course of this grant, and each patent cites grant No. FA9550-14-1-0002 as the source of support.

1. J.G. Eden, S.-J. Park, and K.-S. Kim, "Buried Circumferential Electrode Microcavity Plasma Device Arrays, Electrical Interconnects, and Formation Method," Japanese Patent No. 5,399,901 (November 1, 2013).
2. J.G. Eden and S.-J. Park, "Microdischarge Devices With Encapsulated Electrodes and Method of Making," Japanese Patent No. 5,435,868 (December 20, 2013).
3. P. A. Tchertchian, C. J. Wagner, and J. G. Eden, "Hybrid Plasma-Semiconductor Electronic and Optical Devices," U.S. Patent No. 8,674,461 (March 18, 2014).
4. R. L. Burton, J. G. Eden, S.-J. Park, and D. L. Carroll, "Micro-Cavity Discharge Thruster (MCDT)," U.S. Patent No. 8,689,537 (April 8, 2014).
5. J. G. Eden, J. Gao, and S.-O. Kim, "AC, RF, or Pulse Excited Microdischarge Device and Array," U.S. Patent No. 8,796,926 (August 5, 2014).
6. J. G. Eden, P. A. Tchertchian, T. J. Houlahan, D. J. Sievers, B. Li, and C. J. Wagner, "Flexible Hybrid Plasma-Semiconductor Transistors and Arrays," U.S. Patent No. 8,816,435 (August 26, 2014).
7. J. G. Eden, S.–J. Park, and S. H. Sung, "Ellipsoidal Cavity Microplasma Devices and Powder Blasting Formation," Japanese Patent No. 5,486,002 (February 28, 2014).
8. J. G. Eden, S.-J. Park, M. Lu, and B. Cunningham, "Polymer Microcavity and Microchannel Devices and Fabrication Method," Japanese Patent No. 5,539,650 (May 9, 2014).

9. J. G. Eden, S.–J. Park, M. Lu, and B. Cunningham, “Polymer Microcavity and Microchannel Device and Array Fabrication Method,” U.S. Patent No. 8,864,542 (October 21, 2014).

10. J. G. Eden, S.–J. Park, J. K. Yoon, and B. Chung, “Encapsulated Metal Microtip Microplasma Device and Array Fabrication Methods,” U.S. Patent No. 8,870,618 (October 28, 2014).

11. J. G. Eden, S.–J. Park, T.–L. Kim, and K.–S. Kim, “Microcavity and Microchannel Plasma Device Arrays in a Single, Unitary Sheet,” U.S. Patent No. 8,890,409 (November 18, 2014).

12. J. G. Eden, S.-J. Park, J. H. Cho, and J. H. Ma, “Microplasma Jet Devices, Arrays, Medical Devices and Methods,” U.S. Patent No. 8,957,572 (February 17, 2015).

13. J. G. Eden, S.-J. Park, J. H. Cho, S. H. Sung, and M. H. Kim, “Arrays of Metal and Metal Oxide Microplasma Devices With Defect Free Oxide,” U.S. Patent No. 8,968,668 (March 3, 2015).

14. J. G. Eden, S.-J. Park, J. K. Yoon, and B. Chung, “Encapsulated Metal Microtip Microplasma Devices, Arrays, and Fabrication Methods,” Korean Patent No. 1,515,729 (April 21, 2015).

15. J.G. Eden and J.D. Hewitt, “Dual Channel Pumping Method Laser With Metal Vapor and Noble Gas Medium,” U.S. Patent No. 9,106,052 (August 11, 2015).

16. J. G. Eden and S.-J. Park, “Microdischarge Devices With Encapsulated Electrodes and Its Method of Fabrication, European Patent No. 1,797,579 (August 6, 2015).

17. J. G. Eden, P. A. Tchertchian, C. J. Wagner, D. J. Sievers, T. J. Houlahan, and B. Li, “Flexible and On Wafer Hybrid Plasma-Semiconductor Transistors,” U.S. Patent No. 9,184,341 (November 10, 2015).

18. J. G. Eden, S.-J. Park, J. H. Cho, S. H. Sung, and M.H. Kim, “Arrays of Metal and Metal Oxide Microplasma Devices With Defect Free Oxide”, Korean Patent No. 1,593,291 (February 2, 2016).

19. J. G. Eden and S.-J. Park, “Arrays of Microcavity Plasma Devices With Dielectric Encapsulated Electrodes”, European Patent No. 1,905,057 (March 9, 2016).

20. J. G. Eden, P. A. Tchertchian, C. J. Wagner, D. J. Sievers, T. J. Houlahan, and B. Li, “Hybrid Plasma-Semiconductor Transistors, Logic Devices and Arrays”, U.S. Patent No. 9,263,558 (February 16, 2016).

21. J. G. Eden, P. A. Tchertchian, C. J. Wagner, D. J. Sievers, T. J. Houlahan, and B. Li, “Logic Function Generation From Single Microplasma Transistor Devices and Arrays of Devices,” U.S. Patent No. 9,330,877 (May 3, 2016).

22. J. G. Eden, M. H. Kim, J. H. Cho, and S.-J. Park, “Modular Microplasma Microchannel Reactor Devices, Miniature Reactor Modules and Ozone Generation Devices”, U.S. Patent No. 9,390,894 (July 12, 2016).

23. J. G. Eden, S.-J. Park, J. H. Cho, S. H. Sung, and M. H. Kim, “Gas Reactor Devices With Microplasma Arrays Encapsulated in Defect Free Oxide”, U.S. Patent No. 9,579,624 (February 28, 2017).

24. J. G. Eden, S.-J. Park, J. K. Yoon, and K.-S. Kim, “Phosphor Coating for Irregular Surfaces and Method for Creating Phosphor Coatings”, U.S. Patent No. 9,659,737 (May 23, 2017).

25. J. G. Eden and J. D. Hewitt, “Dual Channel Method for Pumping and Cooling Lasers and Laser Devices”, U.S. Patent No. 9,800,011 (October 24, 2017).

26. J. G. Eden, M. H. Kim, J. H. Cho, and S.-J. Park, “Modular Microplasma Microchannel Reactor Devices, Miniature Reactor Modules and Ozone Generation Devices”, Singapore Patent No. 11201602260S (October 27, 2017).

27. J. G. Eden, M. R. Gartia, and G. L. Liu, “Injection-Seeded Whispering Gallery Mode Optical Amplifier Devices and Networks”, U.S. Patent No. 9,893,486 (February 13, 2018).

28. J. G. Eden, M. H. Kim, J. H. Cho, and S.-J. Park, “Modular Microplasma Microchannel Reactor Devices, Miniature Reactor Modules and Ozone Generation Devices”, South Korean Patent No. 10-1839823 (March 13, 2018).

29. J. G. Eden, S.-J. Park, C. Shin, and A. Mironov, “Hybrid Photochemical/Plasma Reactor Devices”, U.S. Patent Application No. 15/728,986 (November 2019).